Real-time suppression and amplification of neural oscillations using electrical stimulation and phase feedback

David Escobar Sanabria[1], Luke A. Johnson[1], Ying Yu[1], Zachary Busby[1], Shane Nebeck[1], Jianyu Zhang[1], Noam Harel[2], Matthew D. Johnson[3], Gregory F. Molnar[1], Jerrold L. Vitek[1*]

[1] Department of Neurology, University of Minnesota, Minneapolis, MN, USA

[2] Department of Radiology, University of Minnesota, Minneapolis, MN, USA

[3] Department of Biomedical Engineering, University of Minnesota, Minneapolis, MN, USA.

* Correspondence should be addressed to Jerrold L. Vitek (vitek004@umn.edu)

Classification

Biological Sciences/Neuroscience

Keywords

Brain stimulation, closed-loop control, brain circuits, neural oscillations

Author Contributions

D.E.S designed experiments, analyzed the data, and prepared the manuscript; L.A.J., J.Z., and Y.Y. performed surgical procedures; D.E.S., L.A.J., S.N., and Z.B. carried out the experiments; L.A.J., G.M. and M.D.J. contributed to manuscript revisions; N.H. contributed to image (MRI and CT) acquisition and analysis, G.M. and M.D.J. provided logistical support; J.L.V participated in all aspects of the study.

This PDF file includes:

Main Text (Abstract, Significance Statement, Introduction, Results, Discussion, and Methods)
Figures 1 to 5

Abstract

Approaches to predictably control neural oscillations are needed to understand their causal role in brain function in healthy and diseased states and to advance the development of neuromodulation therapies. In this article, we present a neural control and optimization framework to actively suppress or amplify neural oscillations observed in local field potentials in real-time by using electrical stimulation. The rationale behind this control approach is that neural oscillatory activity evoked by electrical pulses can suppress or amplify spontaneous oscillations via destructive or constructive interference when stimulation pulses are continuously delivered at precise phases of these oscillations in a closed-loop scheme. We tested this technique in two nonhuman primates that exhibited a robust increase in low-frequency (8-30 Hz) oscillatory power in the subthalamic nucleus following administration of the neurotoxin MPTP (1-methyl-4-phenyl-1,2,3,6-tetrahydropyridine). The control approach was capable of actively and robustly suppressing or amplifying low-frequency oscillations in real-time in the studied subjects.

Significance Statement

We developed and tested an approach to systematically and predictably control neural oscillations recorded from local field potentials in-vivo by using electrical stimulation. This neural modulation technique is capable of actively suppressing or amplifying neural oscillations with the resolution and time specificity needed to characterize the functional role of oscillatory dynamics in brain circuits. We resolve the experimentally-intractable problem of finding optimal stimulation parameters to suppress or amplify neural oscillations by using subject-specific neurophysiological data and data-driven computer simulations. Together these neural control and optimization approaches allow one to characterize in controlled experiments the role of circuit-level neural oscillations in brain function and study electrical stimulation therapies that predictably modulate brain oscillations.

Introduction

Neuromodulation approaches that predictably control circuit-level neural dynamics in real-time will be of utility in neuroscience to deductively infer causal relationships between controlled changes in these dynamics and brain function. These control approaches could also help identify neural processes causally linked to the manifestation of brain conditions and inform the development of neuromodulation therapies. Neural oscillatory dynamics observed from local field potentials (LFPs) are of particular interest to the development of neuromodulation therapies with feedback given the long-term stability of LFP recordings in cortical and subcortical brain structures in human subjects(1, 2). Evidence from experimental studies and computer simulations suggest that LFP oscillations at low-frequency (<100 Hz) are generated predominantly by synchronized synaptic inputs to neuronal ensembles near the recording site(3, 4). Controlling synchronized synaptic activity in a targeted neuronal ensemble can therefore help modulate information flowing into the target, and thereby influence the information flowing out of the target. Feedback (closed-loop) control systems can drive the dynamics of complex systems to a desired state by adjusting inputs (actuation) based on real-time measurements of the controlled system dynamics (sensing). These feedback control technologies offer the ability to control neural oscillatory activity by using LFP activity as a feedback signal and electrical stimulation for actuation(5).

Current closed-loop stimulation systems deliver isochronal (fixed-frequency) electrical pulses on demand based upon neurophysiological signals extracted from LFP recordings. These on-demand systems have been used in patients with epilepsy(6) and Parkinson's disease (PD)(7) to minimize the amount of stimulation energy delivered to the brain and the likelihood of side effects that may occur with continuous stimulation as a result of current spread beyond the targeted

region. Current on demand systems are, however, not capable of predictively and actively suppressing or amplifying neural oscillatory activity in specific frequency bands and in real-time.

In this study, we developed and tested in-vivo a feedback control framework to actively suppress or amplify spontaneous neural oscillations in real-time by using LFP measurements for sensing and electrical stimulation for actuation. The rationale behind this control approach and our working hypothesis is that damped oscillations evoked by electrical pulses can suppress or amplify spontaneous neural oscillations via destructive or constructive interference when stimulation pulses are continuously delivered at precise phases of these oscillations in a closed-loop scheme. This neural control framework, referred to as phase-locked stimulation, was tested with two parkinsonian nonhuman primates, which exhibited a robust increase in in the power of oscillations in the 8-30 Hz frequency band following administration of the neurotoxin MPTP (1-methyl-4-phenyl-1,2,3,6-tetrahydropyridine), similar to the oscillations observed in PD patients and thought to underlie the development of PD motor signs(8, 9). We were able to actively suppress or amplify STN oscillations in the studied animals by delivering stimulation in the internal segment of the globus pallidus (GPi) phase-locked to oscillations in the STN.. Our experimental data also demonstrate that the mechanism by which phase-locked stimulation exerts its modulatory effect is constructive or destructive interference between low-frequency oscillations evoked by stimulation and the spontaneous oscillations targeted for modulation. Additionally, we developed and validated a methodology to optimize the parameters of phase-locked stimulation and achieve maximum amplification or suppression of neural oscillations. The neural control and optimization approaches presented in this study can be used as a framework to systematically modulate neural oscillatory activity in specific frequency bands in real-time, which could, in turn, be used to control synchronization and coupling of neural circuits.

Results

Spontaneous neural activity can be modulated using oscillations evoked by electrical stimulation. The neural control approach described here provides a framework to modulate low-frequency (<100 Hz) LFP oscillations. The main idea is that low-frequency, damped, oscillations evoked by electrical stimulation of neural tissue can be used to modulate spontaneous inputs to the targeted neuronal ensemble via constructive or destructive interference. See schematic in **Fig. 1a**.

Two nonhuman primates (J and P), rendered parkinsonian with the neurotoxin MPTP, were used to develop and test the phase-locked brain stimulation methodology. These animals exhibited a robust increase in the amplitude of oscillations in the STN in the 8-30 Hz band after MPTP treatment. The power spectral density (PSD) plots of **Figs. 1b,c** show how the power of LFPs in the STN was increased in the parkinsonian condition of the studied animals. These LFPs were created by differentiating potentials at electrode pairs of a deep brain stimulation (DBS) lead located within the STN used for sensing in the closed-loop system. Location of the DBS leads in the STN are shown in **Supplementary Fig. S1**. The frequency bands targeted for modulation were centered at around 11 Hz in animal J and 14 Hz in animal P (**Fig. 1b,c**). Oscillatory modes in these bands were selected because of their high amplitude relative to other oscillatory modes across frequencies. A frequency range of 6 Hz around the targeted center frequencies was selected for the implementation of phase-locked stimulation to allow for variations in the frequency of oscillatory activity while attenuating information outside the frequency band of interest. See Methods for a more detailed description of the signal processing approach.

Electrical stimulation was delivered in the GPi to modulate oscillations in the STN for two reasons. First, large evoked potentials were observed in the STN of both animals when stimulation (bipolar, biphasic) was delivered in the GPi. Second, stimulation in the GPi resulted in smaller stimulation-induced artifacts in the STN than those observed when stimulation was delivered within the STN

itself, facilitating the suppression of artifacts in real-time. The degree of suppression or amplification of neural oscillations achieved using phase-locked stimulation depended upon the amplitude of the stimulation-evoked oscillations in the targeted frequency band. Stimulation-evoked potentials were used as an indirect measurement of the size of neural oscillations evoked by electrical stimulation. Potentials in the STN evoked by stimulation in the GPi are depicted in **Figs. 1d-g.**

By continuously delivering stimulation to the GPi that was phase-locked to oscillations in the STN, we were able to modulate targeted neural oscillations in the STN of both animals. The amplitude of neural oscillations in the targeted frequency bands was a function of the phase angle at which a train of stimulation pulses was delivered (**Figs. 2a-d**). A single pulse was delivered at each oscillatory cycle in animal P, while a train of 3 pulses (165 Hz intra-burst rate) was used in animal J to enhance the modulatory effect of stimulation via temporal summation. The first pulse of the train was aligned to the targeted phase estimate. Our results also show that there are unique phase angles for which maximum amplification or suppression of neural oscillations can be achieved. The lag between angles associated with maximum suppression and amplification was 180 deg. The amplitude of oscillations in the modulated frequency band was significantly decreased (or increased) when stimulation was delivered at the optimal phase for suppression (or amplification) as compared to the amplitude when stimulation was turned off ($p<0.05$). Boxplots that summarize the effect of suppression and amplification of neural oscillations are shown in Fig. 3. The degree of amplification was higher than the degree of suppression in the experiments. One reason for this difference is that stimulation was discontinued when the amplitude envelope of the oscillations was below the 25th percentile threshold (Methods section).

Modulation was local and not artifactual. Artifacts induced by electrical pulses (biphasic, rectangular, 80 us pulse-width) were suppressed in real-time from the LFP data by blanking measurements affected by the artifacts at a sampling rate large enough (~24 kHz) to reconstruct the shape of the artifacts and minimize the effect of antialiasing filters. See the Methods section. In both subjects, the degree of modulation across different contact pairs in different regions inside and outside of the STN was not correlated with the size of the stimulation-induced artifacts, indicating that simulation-induced artifacts did not influence the observed modulation (**Figs. 2c,d**). Evoked potentials measured with electrodes estimated to be within the STN were larger than those outside the STN, suggesting that evoked neural activity was generated by neural sources and sinks located near electrodes located within the STN. Furthermore, spontaneous oscillations in the 8-30 Hz exhibited larger amplitudes inside the STN than outside (OFF state in **Fig. 2c,d**). The degree of amplification or suppression of these spontaneous oscillations achieved using phase-locked stimulation was larger in electrodes located within the STN.

Modulation was mediated by low-frequency evoked oscillations. Short duration (<3 ms) and short latency (<3 ms) components of the evoked potentials, likely associated with antidromic activation of the STN by stimulation of the GPi, were observed in our data (**Figs. 1d,e**), but had a negligible effect on the spectral measurements at low-frequency bands due to their low power in these bands. When the short-duration and short-latency oscillations are blanked in the LFP time series, the modulation presented in **Fig. 2a,b** remains unchanged. The observed modulation (**Figs. 2a-d**) was therefore mediated by stimulation evoked oscillations at lower frequencies.

Optimal modulation parameters can be estimated using data-driven models of the evoked potentials. Finding stimulation phase angles and amplitudes to maximize the amplification or suppression of neural oscillations is a goal for using phase-locked stimulation. This problem is, however, intractable experimentally due to the large parameter space (stimulation phases and amplitudes) and complexity of the experiments. We addressed this problem through mathematical

models of stimulation evoked potentials and steady-state computer simulations of the closed-loop system.

The temporal dynamics of potentials in the STN evoked by stimulation in the GPi (**Fig. 1d,e)** were characterized using linear, time-invariant differential equations and parameterized via system identification techniques(13). A more detailed description of the evoked potential characterization and mathematical models is presented in the **Supporting Information (Stimulation Evoked Oscillations)** and **Supplementary Fig. S2**. Evoked potentials were observed when the stimulation amplitude was greater than or equal to a non-zero value (lower bound). The amplitude of these evoked potentials was a linear function of the stimulation amplitude for stimulation amplitudes greater than the lower bound at which evoked responses occurred. The input-output relationship between the stimulation pulse and evoked potential is accurately characterized by the mathematical models as shown in **Figs. 4a,b** and **Supplementary Fig. S2**. By using the mathematical models of the evoked potentials, numerical simulations were created in which the closed-loop algorithms were evaluated. The numerical simulations incorporated the same algorithms, filters, and time delays present in the real-time control computer to predict optimal stimulation phase angles that suppress or amplify oscillations. In these computer simulations, evoked potential models as well as computer-generated sinusoidal oscillations (synthetic) or previously recorded LFP data were added to obtain the modulated potential.

Simulations of the closed-loop stimulation system and algorithms were created using recorded LFP data in the off-stimulation state to assess whether the mathematical model approximates the experimental data in which phase-locked stimulation was delivered to the animals. A computer simulation of the experiment shown in **Fig. 4d** was created using LFP data in the stimulation-off condition and is shown in **Fig. 4e**. The computer-generated data reproduces the changes in oscillatory power as a function of stimulation phase observed in the in-vivo experiment (**Fig. 4d** vs **Fig. 4e**). This similarity provides evidence of the modulatory role of stimulation-evoked oscillations in the phase-locked stimulation framework. The computer simulations do not reproduce or exhibit stimulation-induced artifacts, further providing evidence that the modulations are mediated by neurophysiological oscillations evoked by stimulation, but not by stimulation-induced artifacts. Discrepancies between simulation and experimental data can be attributed to temporal dynamics and nonlinearities present in the animal neural circuits but not captured in our steady-state computer simulations.

We used sinusoids with an amplitude equal to the mean amplitude of experimentally recorded STN oscillations as a synthetic LFP signal in the computer simulation. Stimulation was delivered at various phase angles (-175, -170, 165, …, 180 deg) and stimulation amplitudes (300, 350….,750, 800 μA) in the computer simulations and a search was performed to calculate the optimal phases and amplitudes that resulted in maximum suppression or amplification of the oscillations in the targeted frequency band. The amplitude envelope of the modulated signal in the targeted frequency band was then used to quantify the degree of modulation achieved using phase-locked stimulation in these computer simulations. The optimal stimulation amplitude to amplify oscillations is equal to the maximum amplitude (upper bound) employed in the search since the size of the evoked potentials is proportional to the stimulation amplitude in both the mathematical models and experimental data(14, 15). The optimal amplitude to suppress oscillations is not necessarily equal to the optimal stimulation amplitude to amplify oscillations since evoked oscillations with high amplitude can create constructive interference even when delivering stimulation at phase angles at which suppression is achieved at lower stimulation amplitudes. A more detailed description of the optimization approach is described in the **Supporting Information (Optimization Approach)**.

We applied the search approach described above to estimate the optimal stimulation phase and amplitude to suppress/amplify 11-17 Hz oscillations in animal P by using one single stimulation pulse. The optimization considered the mean amplitude of the oscillations' envelope measured in the resting, off-stimulation state of the animal. A map of the optimization search, with values of the

mean amplitude of the oscillations' envelope after phase-locked stimulation is applied in the computer simulations at different phases and amplitudes, is shown in **Fig. 5a**. The optimal phase and amplitude to suppress oscillations were found to be 35 deg and 600 μA, respectively. The optimal phase to amplify oscillations at the same amplitude (600μA) was found to be 145 deg. The optimal phase angles for both suppression (35 deg) and amplification (-145 deg) of oscillations at a fixed stimulation amplitude of 600 μA were the same as that found in the experiment depicted in **Figs. 2b** and **Fig. 3c.** These stimulation parameters were used in an experiment with the animal, in which we alternated between maximum suppression and amplification of neural oscillations (**Fig. 5b**). The results of and data shown in **Figs. 2b,d** and **Fig. 5b** validate the search approach utilized to optimize the stimulation parameters and illustrate the capability of phase-locked stimulation to actively suppress or amplify neural oscillations in real-time. The experiments also show that while we attempt to modulate neural oscillations in the 11-17 Hz band, there are also changes in power in higher frequency bands.

Discussion

We developed an experimental approach and optimization framework to systematically and predictably control the amplitude of neural oscillations recorded from LFP data. The neural control approach, referred to as phase-locked brain stimulation, is capable of precisely suppressing or amplifying the amplitude of neural oscillations with the resolution and time-scale required to characterize the functional role of oscillatory dynamics in brain circuits. The optimization framework described in this article to predict phase angles and stimulation amplitudes that maximize the degree of suppression or amplification of targeted neural oscillations resolves a problem that is intractable experimentally. Together these neural control and optimization approaches provide researchers with tools to address fundamental questions regarding the causal role of circuit-level oscillatory dynamics in brain function in healthy and disease states. We used macro-electrode arrays and electrical stimulation waveforms similar to those used in humans chronically implanted with brain stimulation systems for epilepsy and PD, making our modulation approach feasible to study brain function directly in humans.

Modulation mechanisms of phase-locked stimulation. The rationale behind this control framework is that low-frequency oscillations can be actively overwritten (amplified or suppressed) by continuously delivering stimulation pulses at specific phases of the oscillation. The mechanism by which phase-locked stimulation exerts its effect on neural oscillatory activity is likely secondary to its effect on synaptic inputs evoked by electrical stimulation and generated by activation of mono- or multi-synaptic connections to targeted neuronal populations(10, 16–18).

For the experiments carried out in this study, we assumed that both spontaneous and evoked low-frequency oscillations in the STN of the animals were associated with synaptic inputs innervating common STN neuronal ensembles. In our study, we targeted oscillations in the 8-17 Hz band in the STN of two parkinsonian monkeys. The amplitude of oscillations in this band was increased following MPTP administration. The pathophysiological mechanisms by which the amplitude of these oscillations increase in parkinsonian animals and are observed in PD patients is still being debated. Studies with the 6-OHDA mouse model of PD and computer simulations of the human STN indicate that a combination of synchronized inhibitory and excitatory synaptic inputs from the cerebral cortex and the external segment of the globus pallidus (GPe), innervating common neuronal ensembles contributes to the development of these oscillations in the STN(19, 20). In the experiments carried out in this study, we modulated neural oscillations in the STN in the 8-17 Hz band by delivering stimulation in the GPi that was phase-locked to oscillations in the STN. The resultant modulation of oscillatory activity in the STN was mediated by low-frequency, stimulation-evoked oscillations during stimulation in the GPi. These evoked oscillations had sufficient power at the frequencies of the targeted oscillations to create constructive or destructive interference. Although low-frequency damped oscillations in the STN evoked by GPi stimulation

have not been previously characterized, they are likely associated with synaptic inputs to the STN(10, 16–18). Based on known anatomical connections, these evoked oscillations may emerge from a combination of one or more of the following: 1) antidromic activation of GPe followed by activation of collateral branches projecting to the STN(21); 2) orthodromic activation of GPi-PPN-STN pathways, and 3) orthodromic activation of pallido-thalamo-cortico-subthalamic loops. Consequently, controlled changes in the amplitude of STN oscillations achieved via stimulation of the GPi may be mediated by simultaneous synaptic inputs to a number of different neuronal ensembles converging on the STN.

Utility of neural control approach. The neural control framework presented here provides a mechanism whereby one can suppress or amplify neural oscillations in real-time using electrical stimulation. This approach can be employed to deductively infer causal relationships between controlled changes in the amplitude of LFP oscillations, circuit-level brain function, and behavior. This approach can also be leveraged to modulate and characterize the role of circuit-wide neural dynamics in which oscillations are a critical component underlying changes in synchronization and coupling within and across neuronal networks(22, 23). Additionally, we can employ this neural control framework to study how controlled changes in oscillatory dynamics and related changes in circuit-wide neural activity are causally linked to the manifestation of brain conditions. Examples of indications where this neural control framework can be applied are Parkinson's disease and epilepsy. In Parkinson's disease this framework could be used to assess whether synchronization and coupling of low-frequency (5-30 Hz) oscillations throughout the basal ganglia-thalamocortical circuit are linked (directly or indirectly) to bradykinesia, rigidity, gait disorders, or tremor(8, 25). In epilepsy, one could study whether attenuating synchronized epileptiform neural activity can directly or indirectly alter the probability of seizure onset(24). By improving our understanding of causal links between neural circuit dynamics and brain conditions, this closed-loop brain stimulation approach could also guide the development of subject specific neuromodulation therapies delivered based on LFP activity within specific regions of the brain.

From a technological standpoint, the neural control framework presented here is suitable for testing in human subjects because we use LFP activity for sensing and stimulation waveforms that are currently being used in present day neuromodulation devices. LFP data chronically recorded from cortical and subcortical brain structures via macro-electrode arrays have been demonstrated to provide usable neurophysiological information in humans for extended periods of time(26). The experimental setup used in this study, with sensing in the STN and stimulation in the GPi, provides a proof of concept for the implementation of phase-locked brain stimulation. This particular setup, with electrodes in both the STN and GPi, has been implemented in humans(27); however, it is not standard practice as DBS leads are typically implanted in one brain target within the same cerebral hemisphere. In applications in which LFPs are recorded from and stimulation is delivered to the same brain region using a single electrode array (e.g. DBS for PD), hardware and/or software technologies that enable effective and robust artifact removal in real-time are needed to rigorously implement phase-locked stimulation.

Limitations. We assumed that spontaneous and evoked LFP oscillations measured in the STN of the studied animals were associated with synaptic inputs innervating common STN neuronal ensembles. This is a reasonable assumption given that STN neurons simultaneously receive inputs from multiple structures, including the GPe and motor cortex. However, we acknowledge that spontaneous and evoked oscillations may be generated by inputs to adjacent but different populations of neurons, and modulations observed in the experiments may be the effect of the superposition of currents from different neuronal ensembles. Recordings of synaptic activity (postsynaptic potentials) and/or neuronal activity in populations of STN neurons during periods of phase-locked stimulation are needed to understand how this stimulation approach exerts its effect at the cellular level. Although cellular-level mechanisms of modulation are not experimentally addressed in this study, the conceptual framework of phase-locked stimulation, implementation

scheme, and optimization method presented in this article provide proof of concept for this neural control approach. The degree of suppression of neural oscillations achieved using phase-locked stimulation was lower than the degree of amplification because we discontinued stimulation when the amplitude envelope of the targeted oscillations was below a threshold equal to the 25th percentile of this envelope in the off-stimulation condition. This threshold-based approach was implemented to avoid delivering stimulation based on measurements close to the noise floor. A 25th percentile is, however, likely a conservative threshold that may have limited our ability to further suppress oscillations using phase-locked stimulation. Further analysis of optimal threshold selection is needed to improve the modulation effect of this technique. The experimental data shown in **Figs. 2a,b** and **Fig. 5b** indicate that phase-locked stimulation alters oscillatory activity in frequency bands not targeted for modulation. These alterations are, at least in part, due to the power content of the evoked neural activity in frequencies outside the band selected for modulation. Stimulation patterns different to fixed-amplitude pulse trains may be needed to reduce the activation of neural oscillatory activity in frequency bands outside that selected for modulation using phase-locked stimulation. The relative benefit of phase-locked stimulation compared to standard brain stimulation approaches using isochronal stimulation remains to be determined, but the potential utility of this technique for both improving current stimulation therapies and for understanding the pathophysiological basis underlying circuit disorders is compelling.

Materials and Methods

Instrumentation and subjects. All procedures were approved by the University of Minnesota Institutional Animal Care and Use Committee (IACUC) and complied with United States Public Health Service policy on the humane care and use of laboratory animals. Two adult rhesus macaques (female Macaca mulatta) were used in this study, subjects: J (17 years), P (18 years). Each animal was implanted in both the STN and GPi with 8-contact scaled-down versions of human DBS leads (0.5 mm contact height, 0.5 mm inter-contact spacing, 0.625 mm diameter, NuMED, Inc.) as previously described(11). DBS lead locations were approximated using fused pre-implantation MR and post-implantation CT images, histological reconstructions (**Supplementary Fig. 1**), and microelectrode mapping of the STN and GPi prior to implantation of the DBS leads. Data were collected in the normal and parkinsonian state of the animals. The animals were rendered parkinsonian by systemic (intramuscular) and intra-carotid injections of the neurotoxin 1-methyl-4-phenyl-1,2,3,6 tetrahydropyridine (MPTP)(28).

Neural data acquisition and electrical stimulation. Neurophysiological data in the awake-resting state were utilized to characterize how neural oscillations across frequencies changed in the STN from the normal to the parkinsonian condition. Neural data in the resting-awake state were collected using a Tucker David Technologies (TDT, Alachua, FL, USA) workstation with a sampling rate of ~24 KHz. Signals were band-pass filtered (0.5-700 Hz) to extract LFP data and down-sampled to ~3 KHz for analysis. LFPs were created by subtracting potentials from contacts estimated to be within the STN. The use of differential potentials helps minimize the effect of far field potentials and preserve information that is near the recording electrodes. We verified that the animals were alert using video monitoring(11). The power of neural oscillations across frequencies was computed using power spectral densities (PSDs) and the Welch's method. To compute the PSDs, we used 214 points in the fast Fourier transform, a Hamming window of 1.34 sec (¼ 214 points), zero padding (¾ 214 points), and an overlap of 50%. The PSD curves were normalized with respect to the total power, which is the sum of PSD values over all frequencies. The normalized power describes the proportion of power in each frequency band relative to the total power across all frequencies. Analyses were performed using customized scripts in MATLAB (Mathworks, Natick, MA, USA).

Stimulation evoked potentials. We characterized the temporal dynamics of stimulation-evoked potentials in the STN by delivering low-frequency (<4 Hz) anodal and cathodal stimulation to the

GPi, computing stimulation triggered averages of the LFP time series in the STN for both anodal and cathodal stimulation ($X_a(t)$ and $X_c(t)$), and calculating the mean between the anodal and cathodal responses ($(X_a(t) + X_c(t))/2$). This mean evoked response attenuates the stimulation artifacts while preserving the neural evoked potential(14). The amplitude of the stimulation pulses used to characterize evoked potentials and implement the phase-locked stimulation technique in animal J and P was below 800 μA, which was in turn below the stimulation threshold at which we observed side effects associated with activating the internal capsule (e.g. muscle contractions).

Implementation of neural control approach. We implemented phase-locked stimulation using a Tucker David Technologies (TDT, Alachua, FL, USA) neurophysiological recording and stimulation system and a computer fully dedicated to executing signal processing and control algorithms in real-time. LFP data were sampled at ~24 KHz in the neurophysiological recording system, amplified in the +/-10 V range, and transmitted to the control computer via analog channels. The analog signals were digitized in the control computer at ~24 KHz and electrical artifacts were removed from the LFP data by holding for 2.3 ms the value of the LFP sample acquired before the stimulation pulse was triggered. The 2.3 ms holding period was longer than the duration of the artifact but short enough to avoid degrading information recorded at low-frequency. The artifact-suppressed LFP data were then band-pass filtered in the frequency band selected for modulation using second-order Butterworth filters and subsequently down-sampled at ~3 KHz. The instantaneous phase and amplitude of oscillations in the targeted frequency band were estimated using a Hilbert transformer filter(29). The Hilbert filter introduced 16 samples of time delay (5.3 ms) to the closed-loop interconnection, which corresponds to a 23 deg. phase lag relative to the 11 Hz oscillations targeted in animal J and 26 deg. phase lag relative to the 14 Hz oscillations targeted in animal P. A train of stimulation pulses, three for animal J and one for animal P, were delivered at specified phase angles. whenever the amplitude envelope of the oscillations was above the 25th percentile of the envelope computed in the off-stimulation state. Stimulation was turned off when the envelope was below threshold to avoid delivering stimulation based on measurements with small signal to noise ratio. Stimulation was delivered using bipolar, charge-balanced, biphasic, symmetric stimulation pulses with pulse widths of 80 µsec. In the bipolar configuration, the cathode and anode of the stimulation system were connected to separate contacts in the DBS lead located within the GPi. This bipolar configuration was used to minimize the size of artifacts in the recording site. Charge-balanced biphasic pulses were selected to deliver a net zero current and avoid tissue damage (30, 31). The total delay of the closed-loop interconnection, associated with hardware communication was less than 1 ms. This delay was computed as the period between the sample at which the stimulation command was sent from the real-time computer to the stimulation system and the time at which the stimulation artifact was detected in the recordings of the real-time computer. Signal processing and control algorithms were developed using Simulink Real-Time (Mathworks, Natick, MA, USA).

Quantification of neural modulation. We assessed whether the amplitude of neural oscillations changed when phase-locked stimulation was delivered by using scalar measurements of the oscillations amplitude envelope. The scalar measurements are equal to the average of the amplitude envelope over non-overlapping windows of one-second duration. The analytical amplitude of neural oscillations in the targeted frequency band was computed by filtering the raw data in this band, applying the Hilbert transform, and calculating the magnitude of the analytic signal obtained from the Hilbert transform. Pairwise differences between scalar measurements of the oscillations' amplitude in two different conditions were assessed via the Wilcoxon rank-sum test. The p-values resulting from this test were corrected for the number of comparisons via the Bonferroni method. We assumed that the difference between measurements in the two conditions was significant when $p < 0.05$. The comparisons made were stimulation off vs amplification and stimulation off vs suppression.

Acknowledgments

Research reported in this publication was funded by the Wallin Discovery Fund, the Engdahl Family Foundation, the National Institutes of Health, National Institute of Neurological Disorders and Stroke (P50-NS098573, R01-NS037019, R01-NS077657, R01-NS110613, R01-NS094206), the University of Minnesota's MnDRIVE (Minnesota's Discovery, Research and Innovation Economy) Initiative Postdoctoral Fellowships to D.E. and L.A.J. We thank Prof. Tay Netoff for the discussions and suggestions regarding closed-loop brain stimulation techniques. We thank Claudia Hendrix, Devyn Bauer and Ben Teplitsky for their help with histology processing.

References

1. S. J. Hanrahan, *et al.*, Long-Term Task- and Dopamine-Dependent Dynamics of Subthalamic Local Field Potentials in Parkinson's Disease. *Brain Sci* **6** (2016).

2. F. Staub, *et al.*, EP 4. Long term recordings of deep brain activity from the subthalamic nucleus in PD patients using PC+S. *Clinical Neurophysiology* **127**, e176 (2016).

3. G. Buzsáki, C. A. Anastassiou, C. Koch, The origin of extracellular fields and currents — EEG, ECoG, LFP and spikes. *Nat Rev Neurosci* **13**, 407–420 (2012).

4. O. Herreras, Local Field Potentials: Myths and Misunderstandings. *Front Neural Circuits* **10** (2016).

5. S. J. Schiff, T. A. Poggio, T. J. Sejnowski, *Neural Control Engineering: The Emerging Intersection Between Control Theory and Neuroscience* (MIT Press, 2011) (November 4, 2019).

6. M. J. Morrell, RNS System in Epilepsy Study Group, Responsive cortical stimulation for the treatment of medically intractable partial epilepsy. *Neurology* **77**, 1295–1304 (2011).

7. S. Little, *et al.*, Adaptive deep brain stimulation in advanced Parkinson disease. *Ann. Neurol.* **74**, 449–457 (2013).

8. P. Brown, Oscillatory nature of human basal ganglia activity: relationship to the pathophysiology of Parkinson's disease. *Mov. Disord.* **18**, 357–363 (2003).

9. N. J. Ray, *et al.*, Local field potential beta activity in the subthalamic nucleus of patients with Parkinson's disease is associated with improvements in bradykinesia after dopamine and deep brain stimulation. *Experimental Neurology* **213**, 108–113 (2008).

10. P. J. Magill, A. Sharott, M. D. Bevan, P. Brown, J. P. Bolam, Synchronous unit activity and local field potentials evoked in the subthalamic nucleus by cortical stimulation. *J. Neurophysiol.* **92**, 700–714 (2004).

11. D. Escobar, *et al.*, Parkinsonism and Vigilance: Alteration in neural oscillatory activity and phase-amplitude coupling in the basal ganglia and motor cortex. *J. Neurophysiol.*, jn.00388.2017 (2017).

12. A. Devergnas, D. Pittard, D. Bliwise, T. Wichmann, Relationship between oscillatory activity in the cortico-basal ganglia network and parkinsonism in MPTP-treated monkeys. *Neurobiol Dis* **68**, 156–166 (2014).

13. L. Ljung, *System Identification: Theory for the User* (Prentice-Hall, Inc., 1986).

14. A. Romeo, *et al.*, Cortical Activation Elicited by Subthalamic Deep Brain Stimulation Predicts Postoperative Motor Side Effects. *Neuromodulation* **22**, 456–464 (2019).

15. S. Li, G. W. Arbuthnott, M. J. Jutras, J. A. Goldberg, D. Jaeger, Resonant antidromic cortical circuit activation as a consequence of high-frequency subthalamic deep-brain stimulation. *J. Neurophysiol.* **98**, 3525–3537 (2007).

16. I. O. Volkov, Unit responses in the cat auditory cortex to electrical stimulation of nerve fibers innervating receptor cells in different parts of the organ of corti. *Neurophysiology* **14**, 317–323 (1982).

17. K. Kumaravelu, C. S. Oza, C. E. Behrend, W. M. Grill, Model-based deconstruction of cortical evoked potentials generated by subthalamic nucleus deep brain stimulation. *J Neurophysiol* **120**, 662–680 (2018).

18. A. R. Kent, W. M. Grill, Neural origin of evoked potentials during thalamic deep brain stimulation. *J Neurophysiol* **110**, 826–843 (2013).

19. C. J. Wilson, M. D. Bevan, Intrinsic dynamics and synaptic inputs control the activity patterns of subthalamic nucleus neurons in health and in Parkinson's disease. *Neuroscience* **198**, 54–68 (2011).

20. M. D. Bevan, P. J. Magill, D. Terman, J. P. Bolam, C. J. Wilson, Move to the rhythm: oscillations in the subthalamic nucleus–external globus pallidus network. *Trends in Neurosciences* **25**, 525–531 (2002).

21. M. D. Johnson, C. C. McIntyre, Quantifying the Neural Elements Activated and Inhibited by Globus Pallidus Deep Brain Stimulation. *Journal of Neurophysiology* **100**, 2549–2563 (2008).

22. G. Buzsáki, A. Draguhn, Neuronal Oscillations in Cortical Networks. *Science* **304**, 1926–1929 (2004).

23. V. Jirsa, V. Müller, Cross-frequency coupling in real and virtual brain networks. *Front Comput Neurosci* **7** (2013).

24. Jerome Engel Jr.; Timothy A. Pedley, *Epilepsy: A Comprehensive Textbook*, 2nd Ed. (Lippincott Williams & Wilkins, 2008).

25. P. Brown, *et al.*, Dopamine dependency of oscillations between subthalamic nucleus and pallidum in Parkinson's disease. *J. Neurosci.* **21**, 1033–1038 (2001).

26. N. C. Swann, *et al.*, Chronic multisite brain recordings from a totally implantable bidirectional neural interface: experience in 5 patients with Parkinson's disease. *Journal of Neurosurgery* **128**, 605–616 (2017).

27. , Bilateral implantation in globus pallidus internus and in subthalamic nucleus in Parkinson's disease. - PubMed - NCBI (January 23, 2020).

28. T. Hashimoto, C. M. Elder, M. S. Okun, S. K. Patrick, J. L. Vitek, Stimulation of the subthalamic nucleus changes the firing pattern of pallidal neurons. *J. Neurosci.* **23**, 1916–1923 (2003).

29. A. V. Oppenheim, R. W. Schafer, J. R. Buck, *Discrete-time Signal Processing (2Nd Ed.)* (Prentice-Hall, Inc., 1999).

30. R. V. Shannon, A model of safe levels for electrical stimulation. *IEEE Transactions on Biomedical Engineering* **39**, 424–426 (1992).

31. D. R. Merrill, M. Bikson, J. G. R. Jefferys, Electrical stimulation of excitable tissue: design of efficacious and safe protocols. *Journal of Neuroscience Methods* **141**, 171–198 (2005).

Figures and Tables

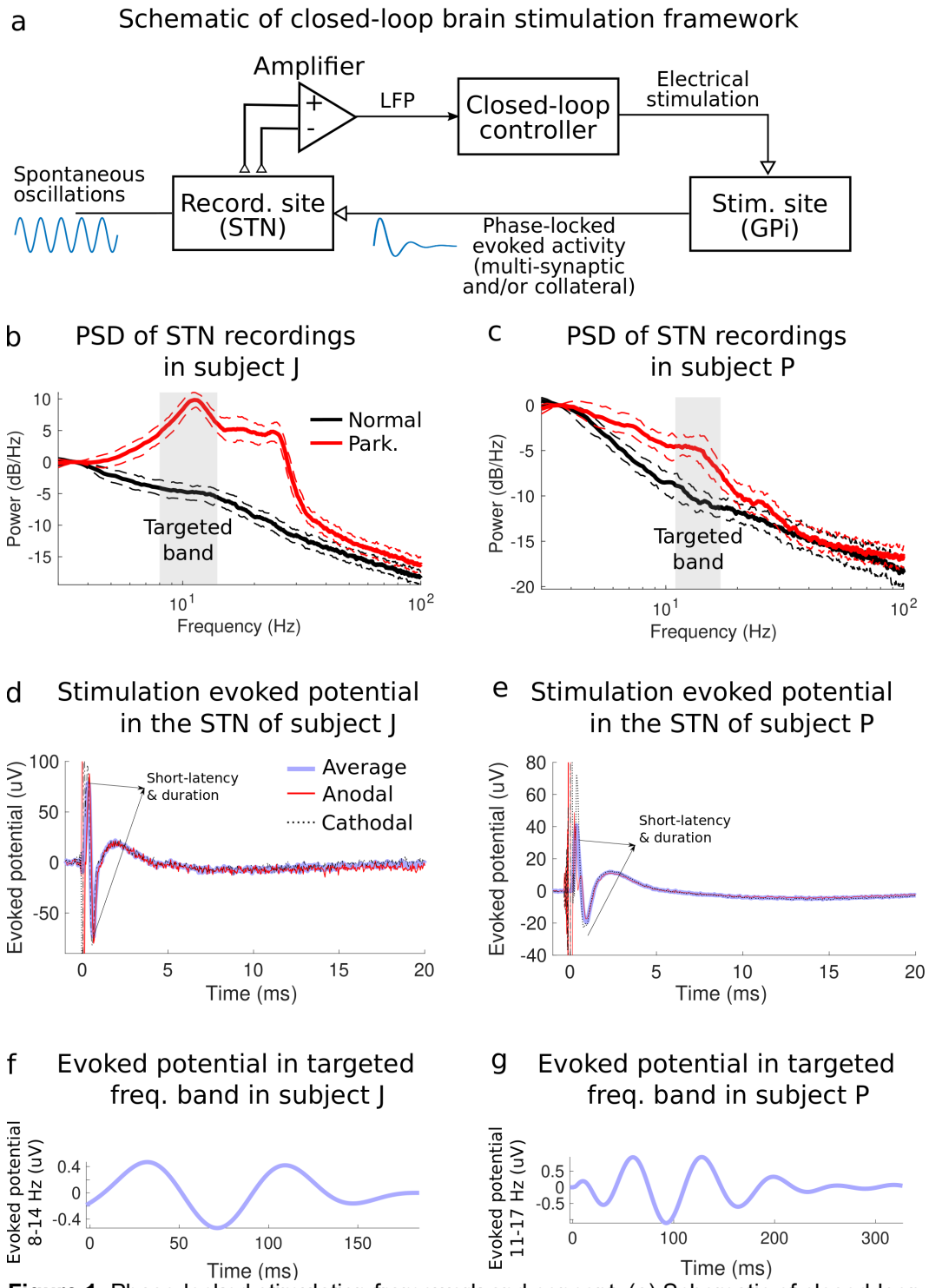

Figure 1. Phase-locked stimulation framework and concept. (a) Schematic of closed-loop neuromodulation framework in which stimulation-evoked activity is used to suppress or amplify spontaneous neural oscillations when stimulations pulses are phase-locked to these oscillations. The power spectral density (PSD) plots of spontaneous LFP recordings in the STN of the studied

animal J and P in the normal and parkinsonian conditions are shown in (b) and (c), respectively. The frequency bands targeted for modulation using phase-locked stimulation are highlighted in gray. These frequency bands have a range of 6 Hz with center frequencies equal to the peak frequency of the PSD plots. Electric potentials in the STN of animal J and P evoked by stimulation pulses in the GPi are shown in (d) and (e), respectively. The evoked potentials displayed in this figure are the average response of a single pulse with an amplitude equal to 600 μA for animal J and 800 μA for animal P. Short-duration and short-latency evoked oscillations, depicted in (d) and (e), are associated with antidromic neural activation of the STN following the stimulus pulse. (f,g) Stimulation-evoked potentials in the targeted frequency bands for animal J and P are shown. The potentials in (f,g) illustrate the evolution of oscillations evoked by a single stimulation pulse in the frequency bands targeted for modulation using phase-locked brain stimulation, responsible for the modulation observed when phase-locked stimulation is delivered. Note that the time scale of the evoked potentials shown in (f-g) is different to that shown in (d-e).

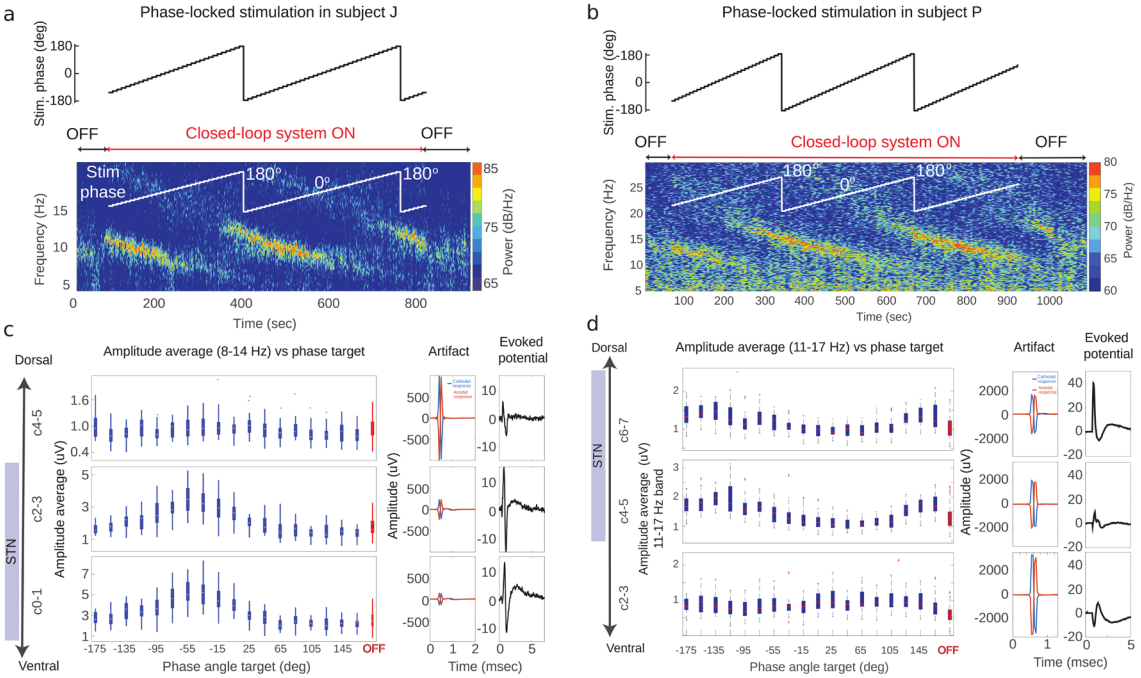

Figure 2. Amplitude of oscillations as a function of stimulation phase. (a, b) Results of experiments in which phase-locked stimulation was tested in animal J and P. The targeted (reference) phase angle for stimulation was varied by 10 degrees every 10 seconds, while the stimulation current delivered to the GPi was fixed at 600 μA in both animals. Spectrograms illustrating the power over time and frequencies for different phase angles in the OFF and ON stimulation state are shown in (a) and (b) for animal J and P, respectively. The spectrograms show data recorded using electrode pairs used to implement the closed-loop stimulation algorithm. The amplitude of neural oscillations as a function of the targeted phase angle and across electrode pairs is shown for animal J and P in (c) and (d), respectively. Electrodes C0-C2 in animal J and C4-C6 in animal P used for sensing are located within the STN. The artifacts and evoked potentials computed across electrode pairs are shown in (c) and (d) (center and right columns). Evoked potentials were calculated based on stimulation-triggered averages of LFPs by using both cathodal and anodal stimulation ($X_a(t)$ and $X_c(t)$). These evoked potentials were calculated as $((X_a(t) + X_c(t))/2)$.

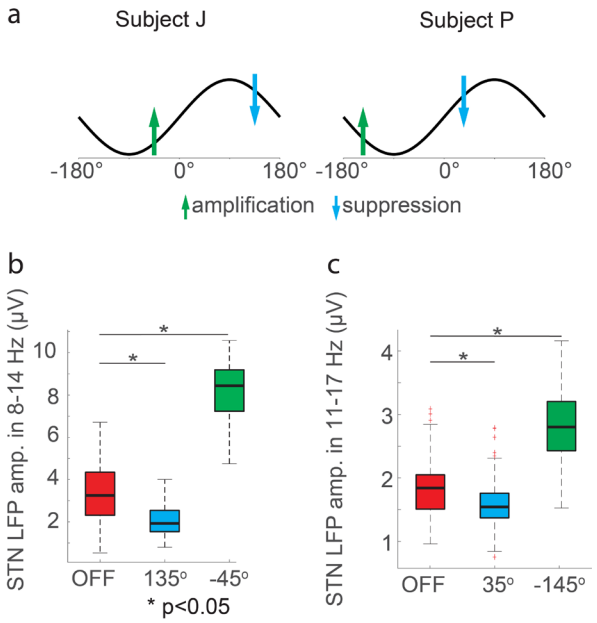

Figure 3. Differences between the amplitude of oscillations when stimulation was OFF and when stimulation was delivered at the phase angles associated with maximum suppression/amplification. (a) Schematic of phase angles at which stimulation was delivered to achieve maximum suppression (blue arrow) or amplification (green arrow) of neural oscillations in the 8-14 Hz band for animal J and 11-17 Hz band for animal P, respectively. (b) Box plots illustrating the interquartile ranges and medians of 1-second segments of the amplitude envelope of LFP data filtered in the targeted frequency band in the OFF stimulation state and when stimulation was delivered at phase angles that achieved maximum suppression and amplification of oscillations. We assumed that the difference between measurements in the two conditions was significant when $p < 0.05$. The p-values resulting from this test were corrected for the number of comparisons via the Bonferroni method. The number of data segments (n) the in the OFF stimulation, amplification, and suppression conditions for animal J were 143, 27, and 18, respectively; for animal P these numbers were 150, 20, and 20, respectively. The boxplots were created based on data from the experiment illustrated in **Fig. 2**.

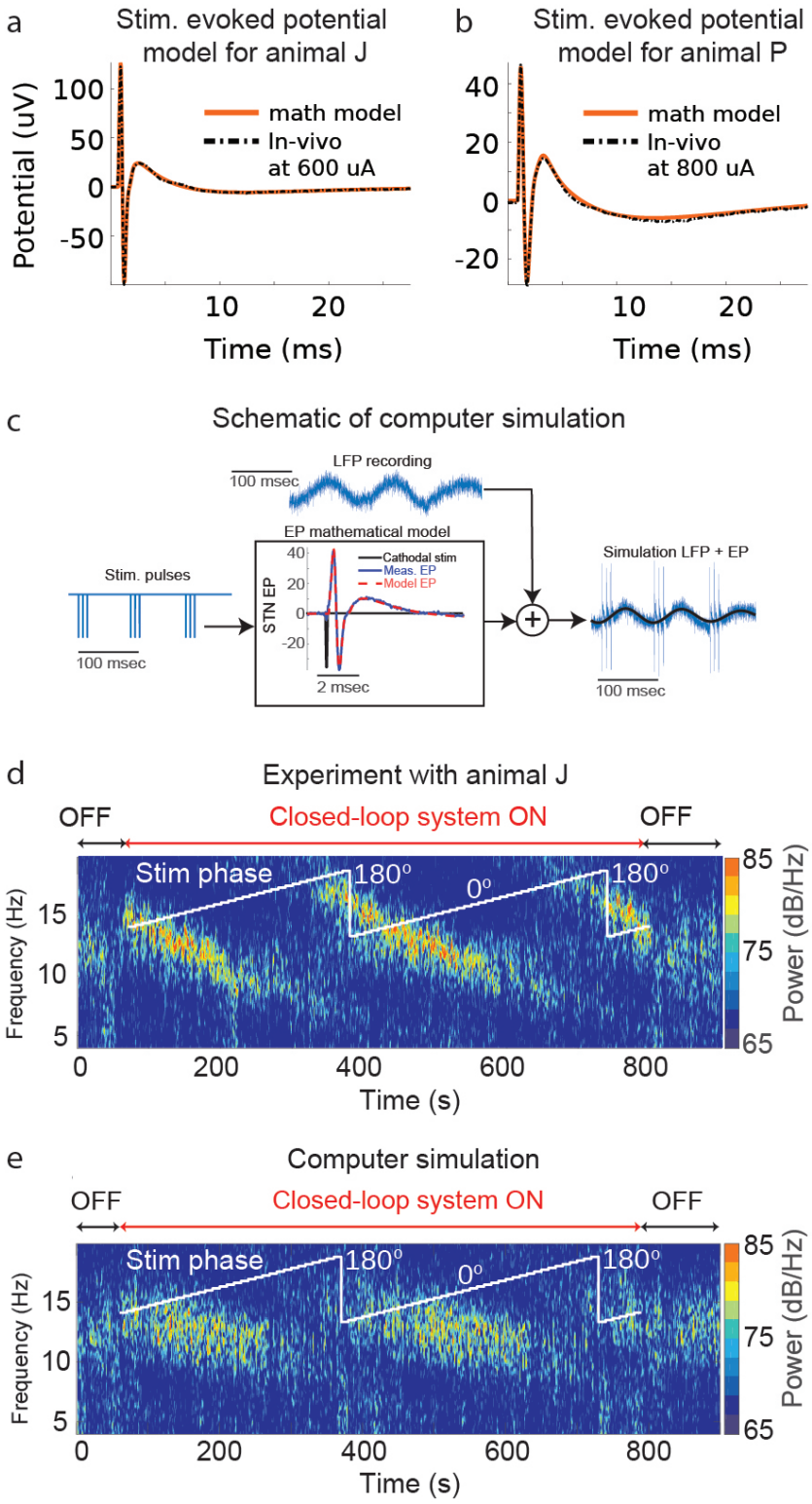

Figure 4. Computer simulations of phase-locked stimulation. (a, b) Stimulation-evoked potentials calculated using experimental data together with their corresponding mathematical models. The evoked potential mathematical models are computed through the convolution of an evoked

potential transfer function obtained via system identification techniques and the stimulation pulse mathematical function. (c) Schematic of computer simulation in which pre-recorded or computer-generated (synthetic) oscillations are added to the evoked potential (EP) time series to model the steady-state of modulated oscillations. The evoked potential time series is computed through the mathematical model with an input equal to stimulation pulses phase-locked to the oscillations in the selected frequency band. (d) Experimental data with animal J in which phase angles were varied over time. (e) Computer simulation of phase-locked stimulation created using STN LFP data (stimulation-free) from animal J and mathematical models of the stimulation-evoked potentials. The targeted phase angles in both experiments and computer simulation were varied over time, increasing the phase angle by ten degrees each ten seconds.

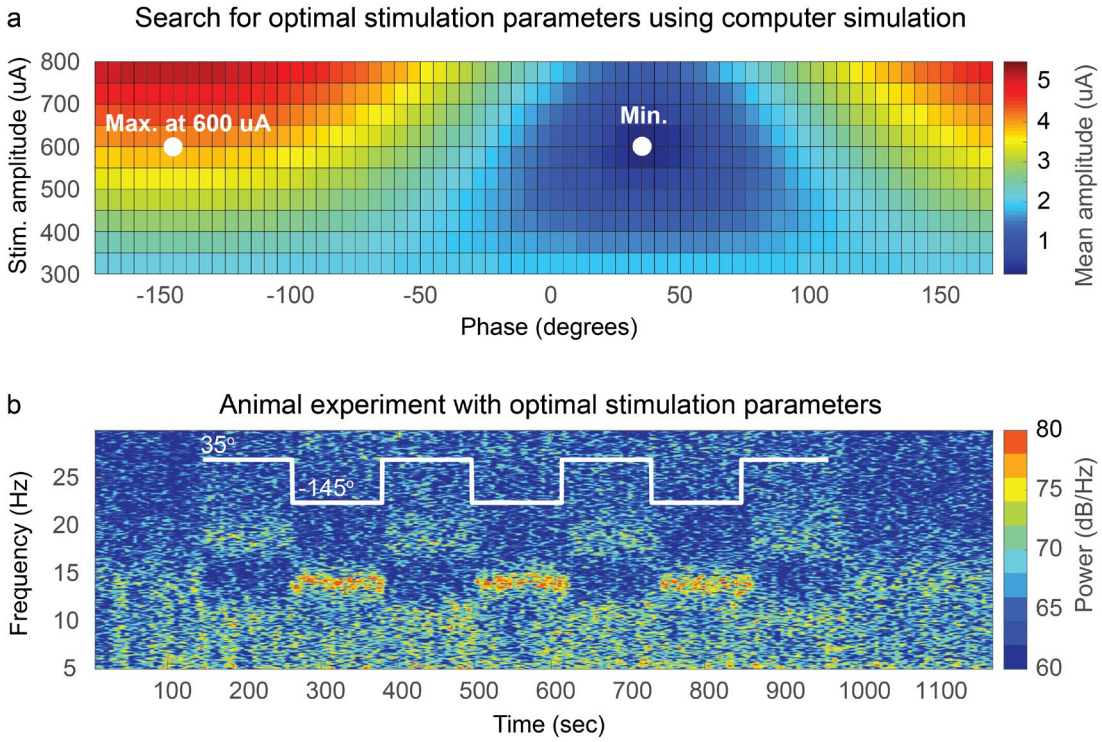

Figure 5. Optimization of stimulation parameters. (a) Optimization map to estimate optimal stimulation amplitudes and phases to suppress/amplify neural oscillations in the 11-17 Hz band with a mean amplitude of 1.95 μA in animal P by using phase-locked stimulation. The color scale represents the mean amplitude of oscillations created in computer stimulations at different stimulation phases and amplitudes. The optimal phase and amplitude to suppress oscillations were found to be 35 deg and 600 μA, respectively. (b) Spectrogram of STN LFP data in which phase-locked stimulation was delivered at stimulation amplitude found to be optimal for suppression of 11-17 Hz oscillations (600 μA). The stimulation phase was alternated between the optimal phase for suppression and the optimal phase for amplification at 600 μA, which is illustrated with the white curve on the spectrogram. The recordings shown in this figure are from the electrode pair that was used for sensing in the closed-loop stimulation system.

Supplementary Information for

Real-time suppression and amplification of neural oscillations using electrical stimulation and phase feedback

David Escobar Sanabria[1], Luke A. Johnson[1], Ying Yu[1], Zachary Busby[1], Shane Nebeck[1], Jianyu Zhang[1], Noam Harel[2], Matthew D. Johnson[3], Gregory F. Molnar[1], Jerrold L. Vitek[1*]

Corresponding author: Jerrold L. Vitek
Email: vitek004@umn.edu

This PDF file includes:

Supplementary text
Figures S1 to S2

Electrode Localization

The locations of the DBS electrode arrays implanted in the STN and GPi were estimated using histological reconstructions in animal J and fused pre-implantation MRI and post-implantation CT images in animal P (Fig. S1). In both animals, identification of target regions prior to implantation of the leads was done using microelectrode recordings and by classifying brain structures based on firing patterns along electrode trajectories. In animal J, electrodes C0 through C2 are within the STN and electrodes C2 through C4 are within the GPi. In this animal, the STN contacts selected for sensing were C0-C2 and the GPi contacts selected for stimulation were C3-C4. In animal P, electrodes C4 through C6 are within the STN and electrodes C3 through C6 are within the GPi. In this animal, the STN contacts selected for sensing were C4-C6 and the GPi contacts selected for stimulation were C4-C6

Stimulation Evoked Oscillations

The amplitude of potentials in the STN evoked by stimulation in the GPi was characterized at three different stimulation amplitudes, in both anodal and cathodal configurations, in each animal (J and P). In both animals, stimulation evoked potentials were not observed for stimulation currents of 100 μA, either in the cathodal or anodal configuration. For stimulation currents of 300 μA and 600 μA in animal J, and 400 μA and 800 μA in animal P, evoked potentials were observed in both anodal and cathodal configurations (**Figs. S2a-f**). The absence of evoked neural activity for stimulation currents at 100 μA indicates that there is a minimum current for which evoked potentials are generated by the electrical stimulation pulses. The evoked potentials generated by anodal stimulation had a phase lag relative to those generated by cathodal stimulation, suggesting that the cathodal phase of the stimulus was responsible for the evoked response (**Figs. S2c,d**). The evoked potentials have a short-latency (<1 ms) and a short-duration (<1 ms) oscillation with peak P1 and trough N1 followed by oscillations of longer duration, including the oscillations with peak P2 and trough N2 (**Figs. S2c-f**).

The input-output relationship between the stimulation pulses and evoked potentials at sample time k were characterized by the following mathematical model

$$y(k) = \begin{cases} [A - \bar{A}]\,(h_e * v)(k) & if\ A > \bar{A} \\ 0 & otherwise, \end{cases} \qquad \text{(Eq. S1)}$$

where h_e is a linear time-invariant transfer function estimated using instrumental variable system identification[19], $v(k)$ is the stimulation input described by the cathodal cycle of the stimulation pulse, the symbol $*$ is the convolution operation, A is the stimulation current amplitude, $\bar{A}$ is the minimum stimulation current for which neural oscillations are evoked. The $A - \bar{A}$ factor is the effective stimulation gain for the linear system model when $A > \bar{A}$. The stimulation waveform is described by the equation

$$v(k) = u(t) - u\left(t - T_{pw}\right)$$

$$u(k) = \begin{cases} -1 & if\ k > 0 \\ 0 & otherwise, \end{cases}$$

where T_{pw} is the pulse width of the stimulation pulse and $u(k)$ the unitary step function. The constant scalar $\bar{A}$ is estimated using experimental data in which evoked potentials are calculated for two different stimulation current amplitudes in a range in which the amplitude of the evoked potentials scales linearly with the stimulation amplitude. Following the model structure of **Eq. S1**,

the evoked potentials generated by stimulation with two different stimulation amplitudes A_1 and A_2 have the following relationship at each sample k

$$\frac{\hat{y}(k,A_1)}{A_1-\bar{A}}=\frac{\hat{y}(k,A_2)}{A_2-\bar{A}}, \qquad (Eq.S2)$$

whenever $A_1>\bar{A}$ and $A_2>\bar{A}$. We used a least squares minimization to estimate $\bar{A}$ based on **Eq. S2** and using evoked potential time series $\hat{y}(k,A_1)$ and $\hat{y}(k,A_2)$ measured experimentally. For doing this estimation, we rearrange **Eq. S2** as follows

$$Y\,\bar{A}=c, \qquad (Eq.S3)$$

where Y is a column vector of the form

$$Y=\ [\hat{y}(1,A_2)-\hat{y}(1,A_1),\hat{y}(2,A_2)-\hat{y}(2,A_1),\dots,\hat{y}(N,A_2)-\hat{y}(N,A_1)]^T,$$

with N being the number of samples of the evoked potential time series. c is a column vector of the form

$$c=\ [A_1\hat{y}(1,A_2)-A_2\hat{y}(1,A_1),A_1\hat{y}(2,A_2)-A_2\hat{y}(2,A_1),\dots,A_1\hat{y}(N,A_2)-A_2\hat{y}(N,A_1)]^T.$$

$\bar{A}$ is abstained via the least squares solution to **Eq. S3**, which is given by $\bar{A}\approx(F^TF)^{-1}F^Tb$.

The values of $\bar{A}$ for animal J and P are equal to 176 μA and 281 μA, respectively. The scaling of evoked potentials by a factor $A-\bar{A}$ is demonstrated in F**ig. S2g-h**. The mathematical model of the evoked potential closely reproduces the evoked potential measurements in both animal J and P (**Fig. S2 i,j**).

The discrete-time transfer functions h_e are described by

$H_e(z)=\frac{b^TZ_b}{a^TZ_a}=\frac{[b_m,b_{m-1},\dots b_1][z^m,z^{m-1},\dots,z]^T}{[a_n,a_{n-1},\dots a_1][z^n,z^{n-1},\dots,z]^T}$, where b is a column vector with real parameters and Z_b a column vector with integer powers of z, the complex frequency representation of a discrete-time, linear, time-invariant system. The vectors a and b obtained via system identification for animal J are

$$a^T=\ [1.0,\ -8.160,\ 29.665,\quad -63.091,86.563,\quad -79.499,\ 48.897,-19.431,4.528,\ -0.472],$$

$$b^T\ =\ 1e-5\cdot[0,\ \ 0.005,\ -0.038,\ 0.123\ -0.231\ \ 0.281\ \ -0.229\ \ 0.121\ -0.038\ \ \ 0.005],$$

and those for animal P are

$$a^T\ =\ \ [1.0,-7.893,27.489,-55.355,70.88,-59.674,\ 32.89,-11.367,2.211,\ -0.181]$$

$$b^T=\ 1e-06\ \ \cdot[\ 0.0005,-0.008,0.06,-0.216,0.416,-0.452,0.2636,-0.061,\ \ -0.009,0.0053].$$

Optimization Approach

We calculate optimal stimulation amplitudes and phases for phase-locked stimulation to amplify or suppress neural oscillations by employing a search approach and the evoked potential mathematical models described in **Eq. S1**. We modeled the spontaneous oscillations and phase-locked evoked potentials as

$$x_{raw}(k,A,\phi)=L\cos(\omega\ k\ T_s)+\sum_{m=1}^{M}\sum_{n=0}^{N}y(k-\left\lfloor\frac{m}{\omega T_s}\right\rfloor-\left\lfloor\frac{\phi}{T_s}\right\rfloor-n\ T_b,A)$$

where ω is the center frequency of the band targeted for modulation, L is the mean amplitude of neural oscillations targeted for modulation and measured in the resting state of the studied subjects. y is the function that characterizes the evoked potential given the stimulation amplitude A and phase ϕ. The term T_s is the sampling period used in the discretization of time and $k = 1,2,\dots,K$, is the sampled time. The term T_b is the intra-burst period of a stimulation pulse train, and N is the number of pulses in each pulse train. In this model, we set $M = \lfloor K\omega T_s \rceil$ pulse trains, considering stimulation for all cycles of the cosine function $L\cos(\omega\, k\, T_s)$ in the interval from $k = 1$ to $k = KT_s$. The operations $\lfloor\cdot\rceil$ and $\lfloor\cdot\rfloor$ are the round and floor functions that transform a real number into an integer.

The component of $x_{raw}(k)$ in the targeted frequency band is given by the equation $x_{fil}(k) = (x_{raw} * h_{bp})(k)$, where $*$ is the convolution operation and h_{bp} is the transfer function of a band-pass filter with cutoff frequencies delineating the targeted frequency band. We used second order Butterworth filters of second order and bandwidth equal to 6 Hz. The focus of our optimization approach is to minimize (or maximize) the amplitude envelope of x_{fil} by selecting a stimulation amplitude A_{opt} and stimulation phase ϕ_{opt}. This optimization is described by the expression

$$\min/\max_{\phi_m, A_q} \frac{1}{K}\sum_{k=1}^{K} Amp(x_{fil}(k)), \qquad (Eq.S4)$$

where $Amp\big(x(k)\big) = |x(k) + jHT\big(x(k)\big)|$, $j = \sqrt{-1}$, HT is the Hilbert transform operator, $|\cdot|$ is the magnitude operation applied to a complex number. The phase angles ϕ_m are discretized between 0 and 2π so that $\phi_m = \frac{2\pi p}{\bar{P}}$, for $p = 0, 1, \dots, \bar{P} - 1$. The number of phase angles considered in our discretization was $\bar{P} = 72$, which leads to an angle resolution of 5 deg. The amplitude of the stimulation current was discretized by $A_q = A_0 + \frac{q(A_Q - A_0)}{Q}$, for $q = 0, 1, \dots, Q$. A_0 and A_q are the lowest and highest values of stimulation amplitude used in the optimization. We used A_0=300 μA and A_Q =800 μA for the optimization carried out for animal P as these currents were above $\bar{A}$ and below the threshold at which side effects associated with activating the internal capsule were observed. Q was set equal to 11, which gives us a stimulation amplitude resolution of 50 μA. The optimal values for the maximization or minimization (**Eq. S4**) were obtained by doing a search over all discretized values of stimulation phase ϕ_p and amplitude A_q.

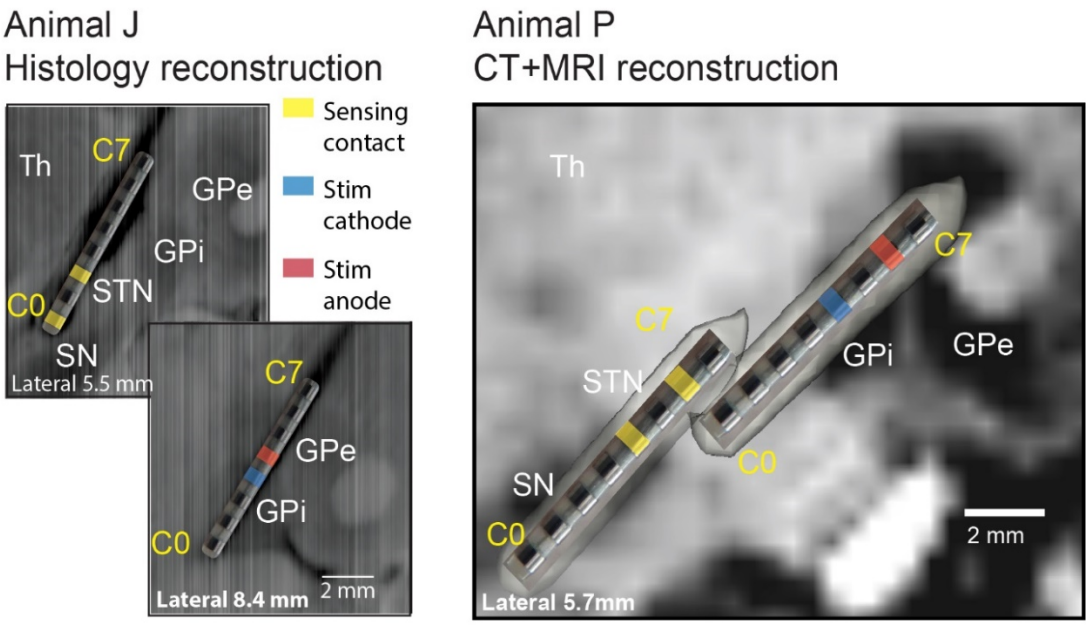

Fig. S1. Localization of DBS electrode arrays used to implement phase-locked brain stimulation in animal J and P. In animal J, histological reconstructions were used to calculate the electrode location. Fused pre-implantation MRI and post-implantation CT images were used for the reconstructions for animal P. The GPi contacts selected for stimulation in the closed-loop system in animal J were C3-4, and in animal P were C4-C6. The STN contacts used for sensing in the closed-loop system were C0-C2 in animal J and C4-C6 in animal P.

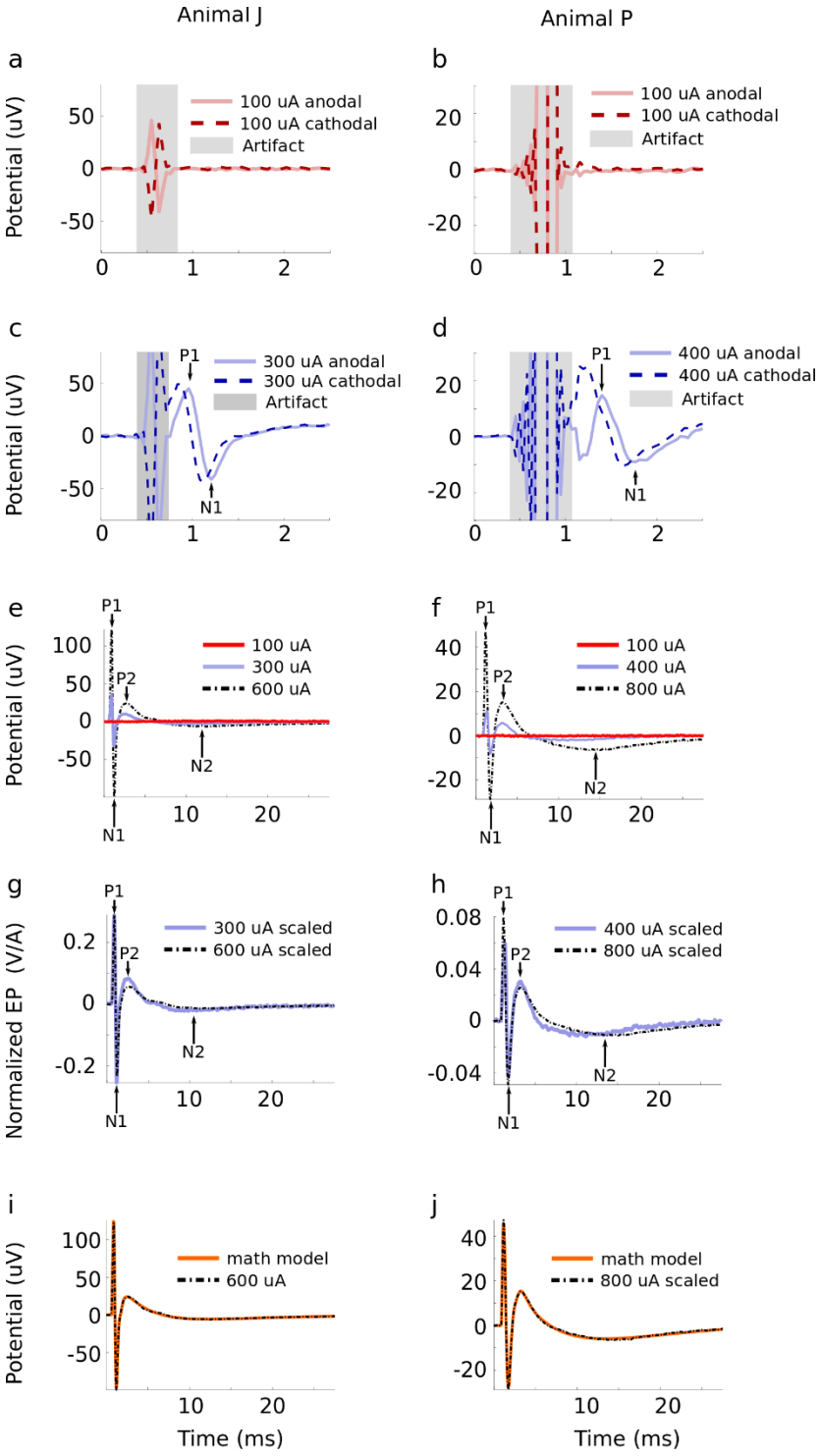

Fig. S2. Characterization and mathematical modeling of potentials in the STN evoked by stimulation in the GPi in animal J and P. (a, b) Sub-threshold potentials for cathodal and anodal stimulation of amplitude 100 μA in both animal J and P. (c, d) Example of super-threshold potentials evoked by cathodal and anodal stimulation with amplitude equal to 300 μA in animal J and 400 μA in animal P. The cathodal response leads the anodal response. (e, f) Evoked potentials generated by stimulation with amplitudes equal to 100, 300, and 600 μA in animal J and 100, 400, and 800 μA in animal P. The peaks (P1, P2) and troughs (N1, N2) of the two first

oscillation cycles are depicted. The evoked potentials are the average response to at least 83 stimulation pulses in animal J and 482 stimulation pulses in animal P for all current amplitudes considered. (g, h) Scaling of evoked potentials by dividing the evoked potentials by the factor $(\boldsymbol{A} - \overline{\boldsymbol{A}})$, where $\boldsymbol{A}$ is the stimulation amplitude and $\overline{\boldsymbol{A}}$ is the minimum current estimated to evoke neural oscillations. The match between the scaled evoked potentials indicate that the scaling approach used in the modeling is accurate to characterize the relationship between the amplitudes of the stimulation pulses and evoked potentials. (i, j) Mathematical models of evoked potentials obtained using system identification techniques shown together with the time series of the evoked potential obtained experimentally in animal J and P.